Journal of
Instrumentation

OPEN ACCESS

Flux-shaping configuration for improved triton burn up detection at the Divertor Tokamak Test facility

To cite this article: Vasiliki Anagnostopoulou *et al* 2025 *JINST* **20** C05035

View the article online for updates and enhancements.

You may also like

- Triton burnup measurements in JET using a neutron activation technique
J. Källne, P. Batistoni, G. Gorini et al.
- Triton burnup measurements and calculations on TFTR
C.W. Barnes, H.-S. Bosch, H.W. Hendel et al.
- Burn-up of fusion-produced tritons and ^{3}He ions in PLT and PDX
W.W. Heidbrink, R.E. Chrien and J.D. Strachan

This content was downloaded from IP address 81.57.8.77 on 03/09/2026 at 14:02

Published by IOP Publishing for Sissa Medialab

Received: *February 18, 2025*
Accepted: *April 14, 2025*
Published: *May 28, 2025*

7th International Conference Frontiers in Diagnostic Technologies
INFN research center of Frascati, Italy
21–23 October 2024

Flux-shaping configuration for improved triton burn up detection at the Divertor Tokamak Test facility

Vasiliki Anagnostopoulou[a,b,*] **Fabio Panza**[a,c] **Giada Gandolfo**,[a] **Andrea Colangeli**,[a] **Michela Gelfusa**[b] **and Daniele Marocco**[a]

[a] *Fusion and Technology for Nuclear Safety and Security Department, ENEA C.R. Frascati, Frascati, Italy*
[b] *Department of Industrial Engineering, University of Rome "Tor Vergata", Rome, Italy*
[c] *National Institute for Nuclear Physics, INFN Genova Section, Genova, Italy*

E-mail: vasiliki.anagnostopoulou@enea.it

Abstract: The measurement of 14 MeV neutrons in deuterium-deuterium plasmas provides insights into triton burn-up and confinement in magnetic fusion devices. At the Divertor Tokamak Test (DTT) facility, triton burn-up neutron yields will be measured by liquid scintillators and single-crystal diamond matrices, which are expected to face saturation-related issues due to low-energy neutron and gamma-ray interference. This work evaluates flux-shaping materials, such as borated polyethylene and lead, to enhance detector performance for the measurement of 14 MeV neutrons in the DTT mixed n/γ field. MCNP simulations are used to model neutron and gamma-ray transport through various material configurations and results show that a combination of a 30%-boron-loaded polyethylene slab followed by a layer of lead can effectively attenuate signals created by low-energy neutrons and gamma-rays while retaining the neutron flux above an energy threshold suitable for 14 MeV neutron measurements. Based on this, a modular configuration is proposed allowing the adjustment of material thicknesses between the different power scenarios of DTT to ensure a flat detector response. The proposed flux-shaping method allows for the insertion of different material combinations in front of each detector, which can extend its operational range by 1–3 orders of magnitude, to simultaneously cover with all three detectors the full spectrum of neutron yield scenarios anticipated at DTT.

Keywords: Neutron detectors (cold, thermal, fast neutrons); Nuclear instruments and methods for hot plasma diagnostics

*Corresponding author.

© 2025 The Author(s). Published by IOP Publishing Ltd on behalf of Sissa Medialab. Original content from this work may be used under the terms of the Creative Commons Attribution 4.0 licence. Any further distribution of this work must maintain attribution to the author(s) and the title of the work, journal citation and DOI.

https://doi.org/10.1088/1748-0221/20/05/C05035

2025 JINST 20 C05035

Contents

1 Introduction 1

2 Investigated materials for n/γ flux-shaping 2

3 MCNP studies of transmission factors 3

3.1 Monoenergetic neutron & gamma-rays 4

3.2 DTT-specific neutron & gamma-ray fluxes 5

4 Results & discussion on detector performance 6

5 Conclusions 8

1 Introduction

As part of the design for the neutron and gamma-ray diagnostic systems of the Divertor Tokamak Test (DTT) facility, it is proposed to add a set of detectors to the Neutron Yield Monitors (NYM) dedicated to time-resolved triton burn-up measurements. These detectors will be placed in a vertical orthogonal module in the DTT Torus Hall at a radial distance of approximately 10 m from the machine axis and will function as neutron counters, with an energy threshold set to distinguish between DD and DT neutrons. The design of the module that will house the NYM diagnostic is ongoing and aims to accommodate various detectors within the available racks while allowing for modular configurations based on the specific needs of each detector, like the insertion of shielding materials of varying thickness on specially designed slots/rails. Details are shown in figure 1.

Candidate detectors include a liquid scintillator (EJ301 type, 1.5 cm diameter and 1 cm thickness) and two single-crystal diamond (sCD) matrices (4.5 mm $\times$ 4.5 mm $\times$ 200 µm and 4.5 mm $\times$ 4.5 mm $\times$ 50 µm), all operating in count mode. Their selection is made to cover a wide neutron yield range, with the scintillator handling yields up to 10^{14} n/s, the thicker sCD from 10^{14} to 10^{16} n/s, and the thinner sCD up to 10^{17} n/s [1]. While all three are sensitive to 14 MeV neutrons, their performance is limited by lower-energy neutrons, gamma-rays, pulse pile-up, and electronic loading, even with data processing techniques like energy thresholding and pulse-shape discrimination.

A promising method to improve measurement statistics is placing flux-shaping materials in front of the detectors to reduce gamma-ray and lower-energy neutron interference while maintaining higher-energy neutron flux [2]. A simple and modular setup is presented here, which could be easily implemented in reality to facilitate the insertion of different shielding materials in various thicknesses. In this work, lead and borated polyethylene of 5% and 30% boron concentration have been studied, which are widely-used for neutron and gamma-ray attenuation respectively. Simulations with the Monte Carlo N-Particle (MCNP) code [3] were used to assess the feasibility of this approach by studying the effect of these materials for various neutron (thermal to 14 MeV) and gamma-ray energies (0.5 MeV–2 MeV), in different material thicknesses and layer configurations.

The material properties are detailed in section 2, simulation results are presented in section 3, while the discussion on extending the detectors' range is in section 4 and the conclusions in section 5.

2025 JINST 20 C05035

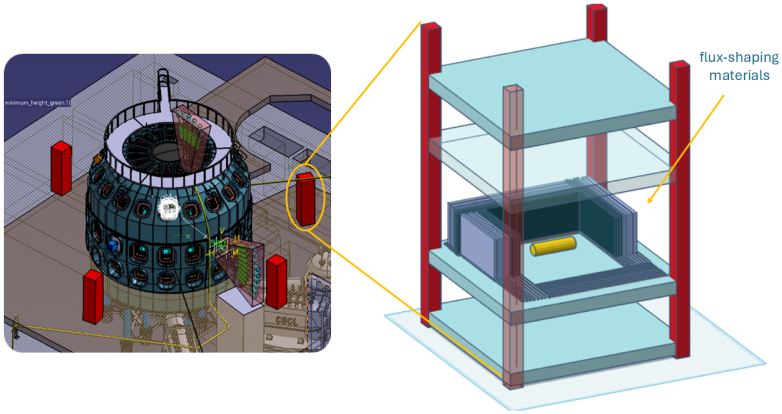


Figure 1. Position of NYM modules in the DTT Torus Hall (left), details of NYM module [4] with modular shielding configurations in linear slots/rails (right).

2 Investigated materials for n/γ flux-shaping

The materials considered in this study are lead (Pb) and borated polyethylene (BPE) with 5% [5] and 30% [6] boron concentration respectively; such selection was mainly guided by the interaction mechanisms of these materials with neutrons and gamma-rays. Polyethylene's hydrogen content effectively scatters neutrons, while boron enhances low-energy neutron absorption due to the high thermal neutron capture cross section of ^{10}B (19.8% of natural boron). Lead on the other hand, as a high-Z material, is known for its gamma-ray stopping capabilities mainly via Compton scattering in a gamma-ray energy range between a few keV and a few MeV. Other important considerations relevant to this application include the fact that BPE and lead are heat resistant up to 80°C and 300°C respectively, can easily be customizable to various sizes, have relatively low cost and are well-studied in shielding applications [7].

Pure lead (100 %) has been considered in this study, since the effect of the small amount of impurities that can be found in commercially available lead (a few % in weigh of Pb) is expected to be negligible. Common lead impurities, like antimony and arsenic, produce secondary gamma-rays via (n,γ) reactions, which have a high cross section for thermal and epithermal neutrons. The final configuration chosen in this application is such that most of these neutrons will be absorbed before impinging on the lead and therefore the flux of secondary gamma-rays is expected to be much lower compared to the total gamma-ray flux. Moreover, the neutron flux above an energy threshold suitable for 14 MeV neutron measurements is practically unaffected, since the (n,γ) reactions have a low cross section in that energy range. Results of simulations performed with 96% lead and 4% arsenic indicate a variation <1% of the transmission factor compared to 100% pure lead.

Other materials were also considered initially but it was decided not to proceed with their selection in this application as simplicity of the geometry was key. The use of cadmium and gadolinium would be effective in the removal of thermal neutrons, however BPE would still be necessary to scatter and moderate higher-energy neutrons of a few MeV. Lead is also necessary to shield against gamma-rays, so this 3-material configuration would not introduce any other benefit other than the potential reduction of the thickness of BPE needed. Other considerations included the fact that gadolinium, while effective at removing thermal neutrons, is significantly more expensive than lead. Cadmium, though also

2025 JINST 20 C05035

effective, is highly toxic and becomes activated by fast neutrons, with ^{115}Cd having a half-life of 53 days, much longer than the activated products of lead. This would pose a significant risk to technicians who would need to enter the Torus Hall and manually adjust the shielding configuration between DTT power scenarios. The final selection of materials to be studied is given in table 1, along with the elemental mass fractions and the densities.

Table 1. Investigated materials, elemental mass fractions (wt.) and densities (g/cm^3).

BPE 5% – 0.918 g/cm^3

Isotope	wt.
^{1}H	0.1314
^{12}C	0.8186
^{10}B	0.0099
^{11}B	0.0401

BPE 30% – 1.28 g/cm^3

Isotope	wt.
^{1}H	0.0968
^{12}C	0.6032
^{10}B	0.0594
^{11}B	0.2406

Lead – 11.34 g/cm^3

Isotope	wt.
^{206}Pb	0.207
^{207}Pb	0.220
^{208}Pb	0.573

3 MCNP studies of transmission factors

To study the effect of these materials on an incoming flux of neutrons and gamma-rays, the transmission factor was used [8], which in essence shows the shielding efficiency of a material (or a set of materials) against the specific radiation studied in each case. This is defined as the ratio between the intensity of the attenuated flux (I) after interaction with a specific target and the unattenuated flux intensity (I_o) impinging on the target:

$$T = \frac{I}{I_0} \tag{3.1}$$

As mentioned in section 1, it is important to study both neutrons and gamma-rays so MCNP6.3 simulations [3] were run separately for each type of radiation, using the ENDF/B-VIII.0 cross section data library [9]. Based on the shape of the NYM modules (see figure 1), a simple geometry was considered consisting of planar monodirectional sources impinging on orthogonal material slabs of 10 cm × 10 cm of various thicknesses. This geometry was selected taking into consideration the orthogonal shape of the NYM modules and the simplicity of inserting and extracting material layers on linear slots/rails to change the thickness of the configuration. The calculation of transmission factors was carried out with the use of the F4 tally, tracking the average number of particles per unit area in the cell normalized per source particle, on two virtual void detectors placed directly before the studied materials and right after them. The simulation with the neutron source was set to track both the neutron interactions and the secondary gamma-rays created, so different F4 tallies were set on the virtual detectors in order to register each type of particle. The same process was carried out separately for the gamma-ray source. In order to avoid an overestimation of the incoming flux due to backscattering in the materials, simulations with no materials were run to determine the direct incoming flux and this was then used in all cases in the calculation of the transmission factor. Figure 2 shows the general configuration in the case of the combination of two materials.

2025 JINST 20 C05035

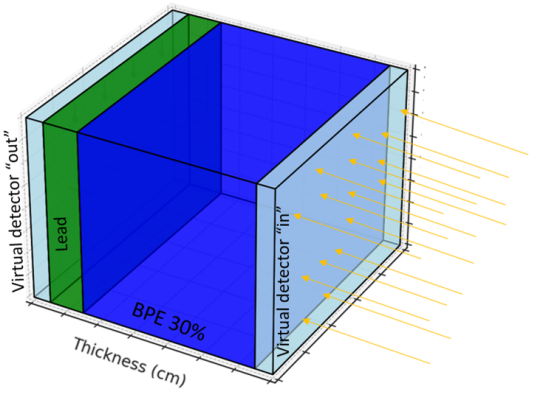


Figure 2. 3D geometry for MCNP, showing materials and virtual "in" and "out" void detectors.

3.1 Monoenergetic neutron & gamma-rays

MCNP simulations with monoenergetic sources and single-material configurations (BPE 5%, BPE 30% and Pb) were run, separately for neutrons and gamma-rays, to guide the selection of materials and thicknesses to be studied in more detail. The neutron energies were selected to cover various orders of magnitude up to 14 MeV: thermal, 1 keV, 0.1 MeV, 1 MeV, 2.45 MeV, 4 MeV and 14.1 MeV. For the gamma-rays, previous MCNP calculations with the DTT 360° model carried out in the past [1] had showed that 80% of the total gamma-ray fluxes at the detector positions had energies below 1 MeV, with most of them around the range of 0.5 MeV, so gamma-ray energies of 0.5 MeV up to 10 MeV were studied. The results of this analysis are shown in figure 3.

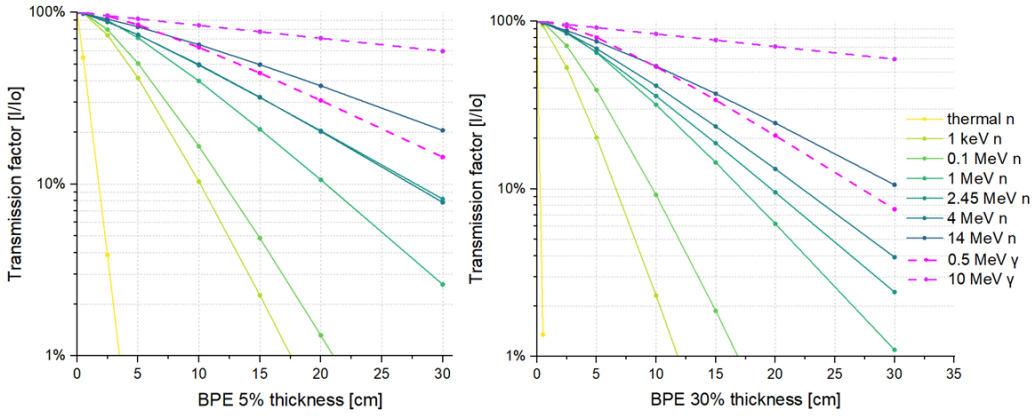


Figure 3. Transmission factor of BPE 5% (left) and BPE 30% (right) vs thickness.

Figure 3 shows that the higher boron concentration in BPE 30% leads to the removal of 99% of the thermal neutrons with a 0.5-cm-thick slab, while BPE 5% needs a thickness of almost 5 cm to achieve the same results. Another observation is that both materials -as expected- prove to be inefficient gamma-ray attenuators. Lead on the other hand effectively shields against gamma-rays of <10 MeV with a few centimeters of material without attenuating the higher-energy neutrons, as shown in figure 4. An important note not evident in the graphs is that low-energy neutrons (up to a few keV) impinging on lead create secondary gamma-rays due to (n, γ) reactions. Based on these

2025 JINST 20 C05035

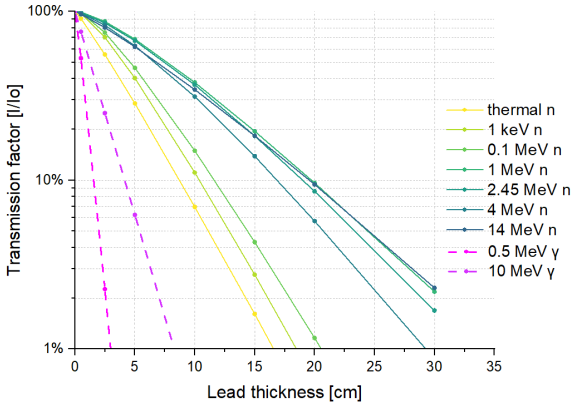


Figure 4. Transmission factor of lead vs thickness.

observations, it was decided to continue the analysis with the study of a combined shield of BPE 30% and lead, which is described in section 3.2.

3.2 DTT-specific neutron & gamma-ray fluxes

The n/γ spectra expected at the detector position in the DTT torus hall (equatorial plane, 10 m radial distance from machine axis) simulated with the 360° MCNP model of the device in a previous study [1] were used as input for a set of simpler MCNP simulations with the geometry described in figure 2. This was done to assess the effectiveness of the candidate flux-shaping materials in the mixed field of neutrons and gamma-rays expected at the detector position. The input data consisted of energy bins and the corresponding flux per source neutron reaching the detector position for two plasma sources, one of 2.45 MeV and one of 14 MeV. To simulate real plasma conditions, these were then scaled accordingly and summed, taking into consideration a conservative scenario of 1% triton burn-up neutrons (TBN) in the overall neutron flux [10]. In case of a higher TBN percentage in the plasma, this will only improve count statistics and not affect the overall analysis.

As mentioned earlier, the detectors are not intended as spectrometers but as neutron counters above an energy threshold selected to reject 2.45 MeV neutrons and maximize counting of events due to 14.1 MeV neutrons (both from the direct and from the scattered component), therefore a threshold of 4 MeV incoming neutron energy has been set for all detectors [1]. The results of the transmission factors for the various geometries are given in table 2, where the goal is to have low transmission factors for total neutrons and gamma-rays and high transmission factors for neutrons above the energy threshold for TBN measurements. It is also important to maintain low levels of secondary gamma-ray production (4^{th} column).

The first two sections of table 2 present simulations with reversed lead and BPE 30% layer orders. Both configurations yield similar transmission factors for total neutrons, neutrons above 4 MeV, and gamma-rays. However when lead is placed first, it generates a high number of secondary gamma-rays, while the BPE-first configuration reduces low-energy neutrons striking lead, minimizing secondary gamma-ray production. Based on this, the suggested layout for the flux-shaping application studied here is to have BPE 30% as a first layer, followed by lead. The remaining table explores various BPE 30% and lead thicknesses to provide different transmission factors, offering flexibility for different power and neutron yield scenarios at DTT, as detailed in section 4.

2025 JINST 20 C05035

Table 2. Transmission factors and secondary γ production for various configurations of BPE 30% and Pb.

Materials & thickness		Total neutrons	Neutrons > 4 MeV	Secondary γ / total flux	Gammas
Pb 2 cm +	BPE 2 cm	52%	77%	7.0%	23%
	BPE 12 cm	6.9%	37%	5.2%	13%
	BPE 30 cm	0.3%	8.0%	0.9%	5.4%
BPE 2 cm		51%	78%	0.2%	24%
BPE 5 cm		27%	64%	0.3%	21%
BPE 12 cm	+ Pb 2 cm	6.6%	38%	0.2%	16%
BPE 15 cm		3.7%	30%	0.2%	14%
BPE 30 cm		0.3%	8.2%	0.0%	8.0%
BPE 1 cm + Pb 10 cm		16%	32%	0.3%	0.8%
BPE 20 cm + Pb 10 cm		0.4%	10%	0.7%	0.4%
BPE 30 cm + Pb 12 cm		0.1%	2.0%	0.2%	0.1%

To showcase the effect of this type of flux-shaping configuration for the mixed n/γ field at DTT, the unattenuated and attenuated neutron and gamma-ray fluxes at the detector positions as simulated with the MCNP 360° model for a total neutron yield of 10^{17} n/s are given in figure 5 for one of the geometries explored (BPE 30% 12 cm + Pb 2 cm). The very high fluxes of thermal neutrons are reduced by several orders of magnitude with this shielding as shown on the left figure, while the neutrons with energies of several MeV present much lower attenuation. Gamma-rays are also sufficiently attenuated.

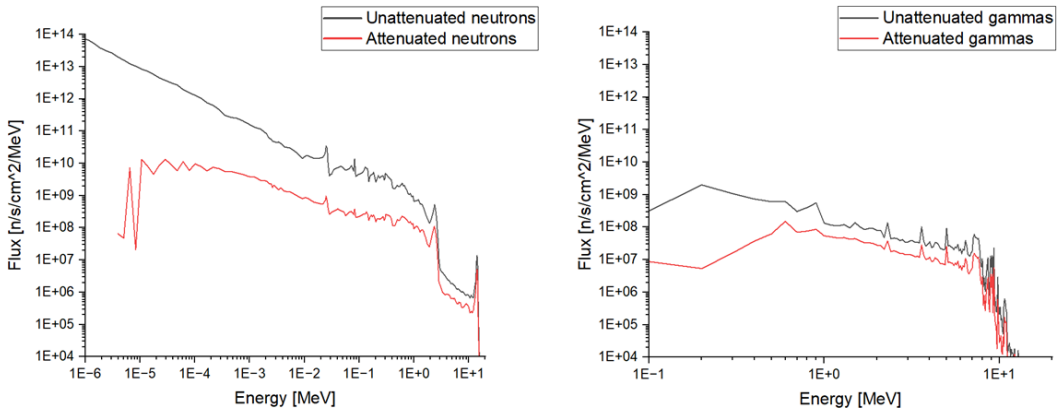


Figure 5. Neutron (left) & gamma-ray (right) fluxes before and after attenuation.

4 Results & discussion on detector performance

The study of the detector performance is based on the requirements on total count rate and the number of counts above the 4 MeV energy threshold (see section 3.2) set to discriminate between noise and the TBN component, which is the desired measurement in this case. To avoid saturation during the measurement process, the detectors should operate with a maximum total count rate around 1 Mcps (10^6 counts/s). At the same time, a goal of 10^3 counts above the neutron energy threshold is set in order to ensure a maximum statistical error in the counts of 3%.

2025 JINST 20 C05035

The count rate is then calculated using the flux arriving at the detectors (estimated via MCNP) for different values of DTT neutron yield, the detector area and the counts per neutron of the detectors as reported in [1]. Based on these requirements, without shielding the liquid scintillator operates up to a total neutron yield of 10^{14} n/s, the 200-mµm-thick sCD up to 10^{16} n/s and the 50-µm-thick sCD up to 10^{17} n/s, as illustrated in figure 6. The time resolution required to achieve a total of 10^3 counts above the energy threshold selected for TBN measurements is shown in the right graph up to the DTT neutron yield where each detector can operate without saturation issues, so the time resolution values are omitted for the liquid scintillator and for the 200-µm-thick sCD in the higher DTT neutron yields.

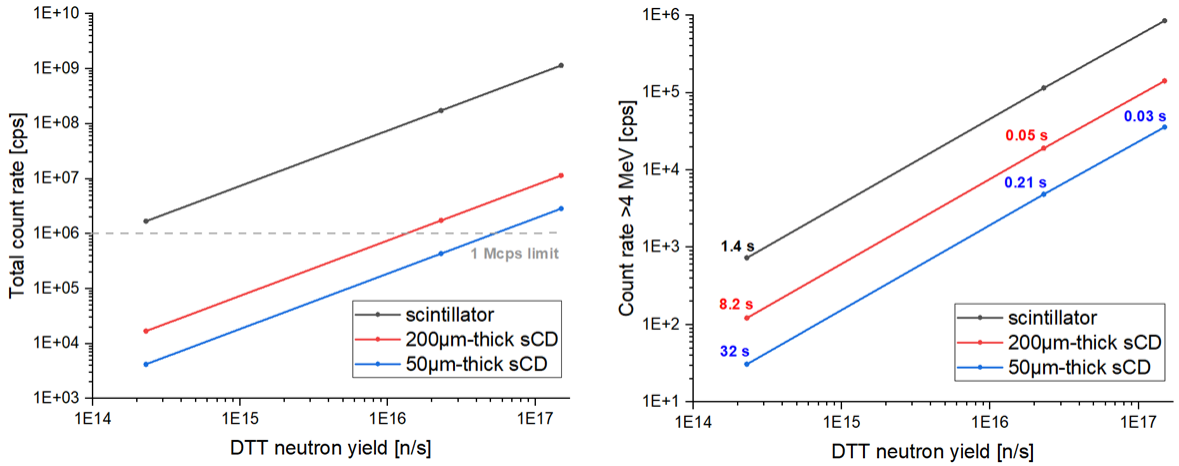


Figure 6. Count rate without flux-shaping materials vs DTT neutron yield. Total count rates (left) and count rates above 4 MeV neutron energy threshold (right).

If appropriate flux-shaping materials are placed in front of the detectors, it is possible to extend their operational range in order to have redundancy in the measurements. Table 3 reports three different flux-shaping configurations that can be used to enable the simultaneous operation of the three detectors over the full range of the expected DTT neutron yield.

Table 3. Flux-shaping configurations for various DTT neutron yields.

Detector	**Configuration nomenclature**		
	A	B	C
Scintillator	BPE 30% 2 cm + Pb 2 cm	BPE 30% 20 cm + Pb 10 cm	BPE 30% 30 cm + Pb 12 cm
200-µm-thick sCD	no attenuation	BPE 30% 1 cm + Pb 2 cm	BPE 30% 12 cm + Pb 2 cm
50-µm-thick sCD	no attenuation	no attenuation	BPE 30% 5 cm + Pb 2 cm

Performances in terms of total count rate and count rate above the energy threshold are reported in figure 7, which suggests that all three detectors can operate within the required range for the entire DTT neutron yield if the material configurations listed in table 3 are used for each detector. This setup is easily achievable, as the detectors will be placed in a vertical module that allows for different materials to be positioned in front of each one. The right graph of figure 7 shows the count rate for neutrons

2025 JINST 20 C05035

above the energy threshold selected for TBN measurements and the respective time resolutions for the various DTT neutron yields, when the designated flux-shaping materials are used. In this case, it is possible to extend the operational range of the liquid scintillator and of the 200-µm-thick to cover the entire expected neutron yield without having a negative effect on the time resolution of the detectors.

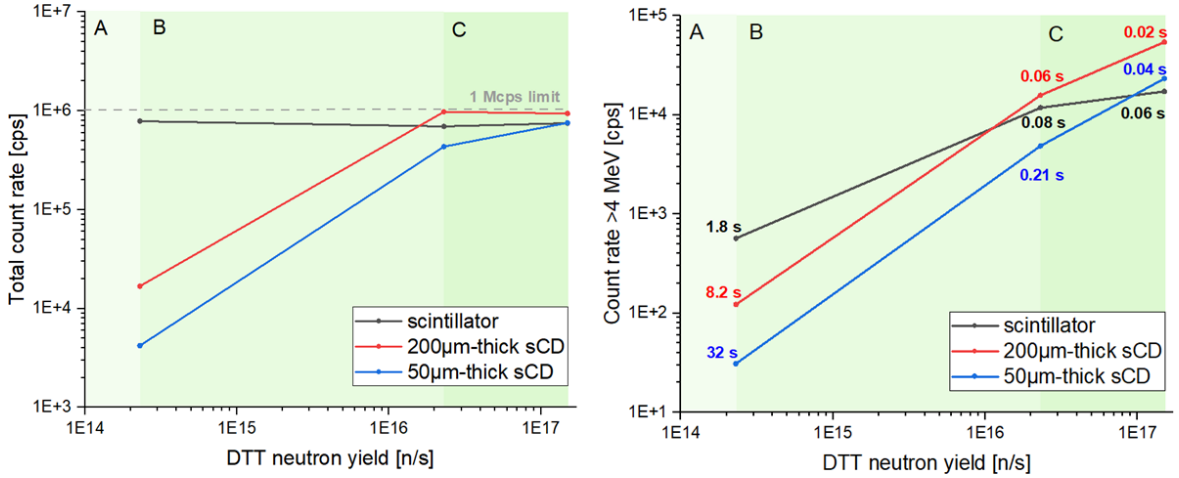


Figure 7. Count rate with flux-shaping materials vs DTT neutron yield. Total count rates (left) and count rates above 4 MeV neutron energy threshold (right).

5 Conclusions

In this study, the use of flux-shaping materials to enhance the performance of neutron detectors dedicated to triton burn-up measurements at the Divertor Tokamak Test (DTT) facility was investigated. MCNP simulations demonstrated that a combination of borated polyethylene and lead effectively reduces the interference from low-energy neutrons and gamma-rays while preserving the high-energy neutron flux. A modular configuration is proposed that ensures flexibility to adapt to varying DTT operational scenarios by modifying the thickness of the materials. The recommended shielding arrangement —BPE 30% followed by lead— minimizes secondary gamma-ray production and extends the operational range of the liquid scintillator and of the 200-µm-thick diamond detector by 1–3 orders of magnitude. This solution enables reliable measurements across the full spectrum of anticipated neutron yields while maintaining a flat detector response and preventing saturation. Future work will focus on the detailed design of the shielding configurations for each detector, along with new simulations incorporating the materials directly into the MCNP DTT 360° model to verify these results with the detectors positioned in the NYM racks and exposed to the plasma conditions expected during the operation of the tokamak.

2025 JINST 20 C05035

References

[1] D. Marocco et al., *Neutron Yield Monitors for the Divertor Tokamak Test (DTT) facility: detector set, expected performance and integration*, presented at *33rd Symposium on Fusion Technology (SOFT 2024)*, Dublin City University, Ireland, 22–27 September 2024, submitted for publication at *Fusion Eng. Des.* (2024).

[2] X. Wang et al., *Neutronics simulations for the design of neutron flux monitors in SPARC*, *Rev. Sci. Instrum.* **95** (2024) 083560.

[3] J.A. Kulesza et al., *MCNP® Code Version 6.3.0 Theory & User Manual*, Tech. Rep. LA-UR-22-30006, Rev. 1, Los Alamos National Laboratory, Los Alamos, NM, U.S.A. (2022).

[4] R. Abburi, M. Praveena and R. Priyakanth, *TinkerCad — A Web Based Application for Virtual Labs to help Learners Think, Create and Make*, *J. Eng. Educ. Transform.* **34** (2021) 535.

[5] MarShield Radiation Shielding, *Borated polyethylene neutron shielding*, (2024), https://marshield.com/borated-polyethylene-neutron-shielding.

[6] YS Plastics, *30% borated polyethylene*, (2024), https://www.ysplastics.com/30-borated-polyethylene/.

[7] J.C. Liu and T.T. Ng, *Monte Carlo calculations using MCNP4B for an optimal shielding design of a 14-MeV neutron source*, *Radiat. Prot. Dosim.* **83** (1999) 257.

[8] G. Almisned, G. Susoy and H.O. Tekin, *Neutron transmission analysis in borated polyethylene, boron carbide, and polyethylene: Insights from MCNP6 simulations*, *Radiat. Phys. Chem.* **218** (2024) 111585.

[9] D.A. Brown et al., *ENDF/B-VIII.0: The 8th Major Release of the Nuclear Reaction Data Library with CIELO-project Cross Sections, New Standards and Thermal Scattering Data*, *Nucl. Data Sheets* **148** (2018) 1.

[10] R. Villari et al., *Nuclear design of Divertor Tokamak Test (DTT) facility*, *Fusion Eng. Des.* **155** (2020) 111551.

2025 JINST 20 C05035